



Heat transfer enhancement by natural convection in a partially porous annular space between two coaxial cylinders saturated by Cu–water nanofluid

Youness Foukhari^a, Mohamed Sammouda, Mohamed Driouich

Laboratory of Research in Physics and Engineering Sciences, Polydisciplinary faculty, Sultan Moulay Slimane university, Beni Mellal 23000, Morocco

Received: 12 October 2022 / Accepted: 10 February 2024

© The Author(s), under exclusive licence to Società Italiana di Fisica and Springer-Verlag GmbH Germany, part of Springer Nature 2024

Abstract The aim of this research is to investigate heat transfer by free convection in an annular, partially porous space between two coaxial cylinders with a permeable interface saturated by (Cu–water) nanofluid. The inner cylinder of the enclosure is kept at a constant hot temperature, while the outer is kept at a constant cold temperature. The base walls are impermeable and insulated. A finite difference-based vorticity-stream function approach is used to solve the nonlinear coupled conservation equations with prescribed boundary conditions, whereas the Successive Over Relaxation algorithm is used to solve the stream function equation. The obtained numerical results in terms of streamlines, isotherms, and heat transfer rate expressed by the Nusselt number are presented to demonstrate the effect of various control parameters, such as the Rayleigh number $10^4 \leq Ra \leq 10^6$, Darcy number $10^{-5} \leq Da \leq 10^{-2}$, porosity $0.1 \leq \epsilon \leq 0.9$, nanoparticles concentration $0.01 \leq \phi \leq 0.05$ and the effective thermal conductivity. They showed that the increase in the Ra number and nanoparticle concentration causes an improvement in thermal energy transmission across the active wall. Also, the increase in the Da number makes the medium more permeable, which means more freedom for nanofluid to move. The results also show a significant effect of the porous layer thickness on the fluid flow pattern and the rate of thermal energy transport. Furthermore, this study demonstrates that there is a critical value of porosity for a given nanoparticle concentration for better heat transfer enhancement. Nonetheless, the purpose of this research could be to better understand the behavior of the nanofluid in this specific configuration, as well as to understand how other characteristics like porosity and porous layer thickness might influence heat transfer and fluid flow characteristics. This knowledge will be useful in a variety of industrial and technological applications where heat transfer efficiency is critical.

List of symbols

| | |
|--------------------|----------------------------------|
| AL | Aspect ratio |
| R_i | Inner radius |
| R_e | Outer radius |
| H | Cavity height |
| g | Gravity acceleration |
| r, z | System coordinate |
| \bar{r}, \bar{z} | Dimensionless coordinate |
| T | Temperature function |
| \bar{T} | Dimensionless temperature |
| U, W | Velocity component |
| \bar{U}, \bar{W} | Dimensionless velocity component |
| K | Porous medium permeability |
| Da | Da number |
| Pr | Prandtl number |
| Ra | Rayleigh number |
| Nu_{ave} | Average Nusselt number |
| Nu_{loc} | Local Nusselt number |
| C_p | Specific capacity |
| Σ, Λ | Nanofluid constants |
| β | Thermal expansion coefficient |

^a e-mail: youness.foukharifpb@usms.ac.ma (corresponding author)

| | |
|----------------|-------------------------------|
| λ | Thermal conductivity |
| ϕ | Nanoparticle concentration |
| μ | Dynamic viscosity |
| ρ | Density |
| Γ | Effective viscosity |
| α | Thermal diffusivity |
| Ω | Vorticity function |
| $\bar{\Omega}$ | Dimensionless vorticity |
| $\bar{\Psi}$ | Dimensionless stream function |

Subscripts

| | |
|------------|---------------------|
| p | Porous medium |
| nf | Nanofluid |
| eff | Effective |
| c | Cold |
| h | Hot |
| b_f | Base fluid |
| n_p | Solid nanoparticles |
| ϵ | Porosity |

1 Introduction

Thermal energy transport improvement in energy devices has received significant attention for its importance and direct implication in many engineering applications and has been studied widely in the last decade in the literature. Many researchers have considered nanofluids as a working medium for the simple reason that the presence of nanoparticles boosts the thermal conductivity of the mixture, making it a viable candidate for heat removal techniques. It is one of the best solutions, which was discovered for the first time by Choi et al. [1].

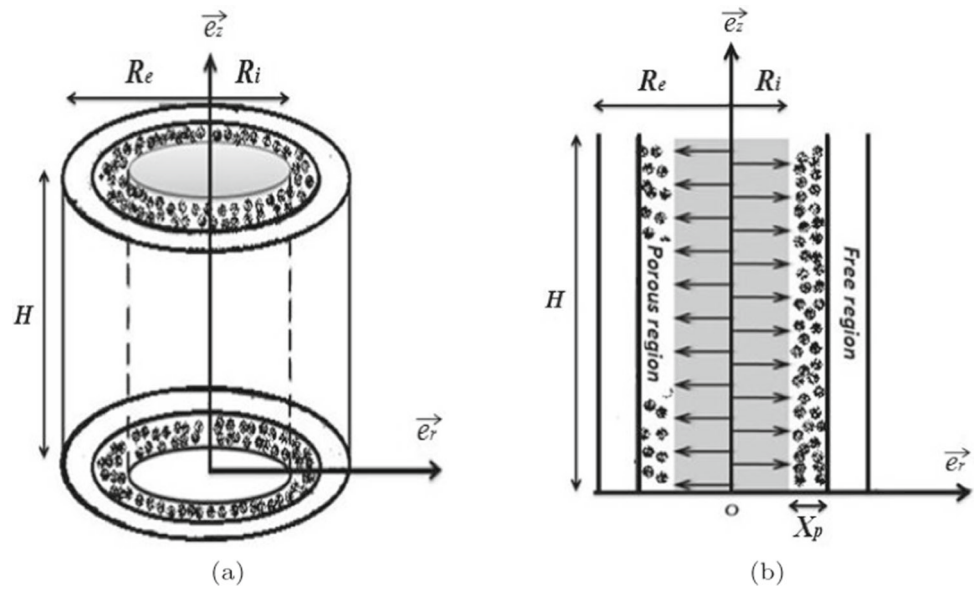
In addition to employing nanofluids, we discovered that there is another alternative, depicted in a mixture of various mediums. It depicts a confined area that has been partially filled with a porous layer with a permeable interface and saturated by a nanofluid, which can be divided vertically or horizontally depending on the applications. Numerous industrial and environmental applications call for these techniques. Among the uses are fuel cells, solar collectors, and fibrous thermal insulation. Beavers and Joseph [2] made the first attempts to analyze natural convection flow heat transfer between a porous medium and a homogeneous fluid experimentally and analytically by focusing on the boundary condition at the fluid/porous interface. Li and Hu [3, 4] investigated the impacts of stress jump, stress continuity, and thermal interface conditions at the fluid-porous interface of a channel, which was partially filled with porous media. According to the results, for larger Darcy numbers and stress jump coefficients, the Nusselt number anticipated by the stress jump condition differs somewhat from the value predicted by the stress continuity condition. Hu and Li [5] investigated the effects of the partially porous medium under forced convection conditions analytically, and the porous medium was modeled using the Darcy-Brinkman technique. They found precise temperature distribution solutions for both local thermal non-equilibrium (LTNE) and local thermal equilibrium (LTE) conditions. They looked at both solid and fluid heat sources and discovered that having extra source terms caused singularities in the Nusselt number. They discovered more than one singularity when the porous filling ratio was raised. In a rectangular enclosure, Mehryan et al. [6] explored the conjugate natural convection flow and heat transfer of hybrid nanofluids. Alsabery et al. [7] investigated the Darcian natural convection of a nanofluid in a trapezoidal cavity partially filled with porous media numerically. The inclusion of silver-water nanofluid boosted convection heat transfer considerably, and the heat transfer rate was controlled by the inclination angle of the cavity. The distinction between two main types of fluid flow interfacial conditions, which are depicted in clear fluid and porous medium, is investigated by Rashidi et al. [8]. Chamkha and Ismael [9] used the Darcy-Brinkman model to tackle the problem of a differentially heated and vertically partly stratified porous cavity filled with nanofluid via natural convection. Sheremet et al. [10] reported the results of a numerical study of natural convection and heat transfer within a horizontal concentric annulus filled with a porous medium and saturated with a Cu–water nanofluid. This study investigated the effects of the Rayleigh number, porosity of the porous medium, radius ratio, and the media's solid matrix (glass balls and aluminum foam) on the Nusselt number and flow regime. Karimi et al. [11] investigated the forced convection in a channel partially filled with a porous material and exposed to a constant wall heat flux analytically. Mahmoudi et al. [12] looked at the heat behavior of a channel with a porous layer in the middle. The results revealed that an ideal porous thickness of 0.8 will optimize the Nusselt number with a suitable pressure drop under model A, which more closely resembles the LTE model than model B. Additionally, the impact of inertia factors on heat transmission under models A and B was explored. Astanina et al. [13] investigated numerically free convection in a square cavity with two adhering porous blocks in the center. The obtained results revealed that the

Darcy number improves heat transfer at the hot wall, but increasing the size of the porous layers reduces the heat transfer rate at this hot wall. Chamkha and Ismael [14] analyzed the conjugate free convection-conduction heat transfer in a square domain formed of a porous cavity filled with nanofluids and heated by a triangle solid wall. Their findings suggested that heat transfer enhancement occurred when the wall thickness was greater than a critical value and that this critical value grew as the Rayleigh number rose. By using Buongiorno's model, Tahmasebi et al. [15] investigated the natural convection heat transfer in a cavity filled with three layers of solid, porous medium, and free fluid. Yang et al. [16] compared the effects of the stress-jump condition and the B-J condition on the fluid flow in a partially filled porous channel under the Darcy model and the Brinkman-extended Darcy model and looked into the errors for the interface velocity, predicted by the velocity slip coefficient and the stress jump coefficient. Torabi et al. [17, 18] derived semi-analytical solutions for temperature profiles and the Nusselt number using the LTNE model to investigate thermal performance, including entropy generation, in a partly porous channel. Saryazdi et al. [19] demonstrated that raising the particle volume fraction increases the Nusselt number. Furthermore, wall shear stresses are enhanced. Under the LTNE model, five temperature conditions with a slip velocity condition for the porous-fluid interface were examined by Yang and Vafai [20]. Bendaraa et al. [21] studied the problem of natural convection in an inclined square cavity filled with a Cu/water nanofluid under a differentially heated configuration in the presence of a magnetic field that tracks the cavity in its inclination. Foukhari et al. [35] evaluated free convection in a coaxial cylinder enclosure filled by a porous medium and filled by a nanofluid using various nanoparticle shapes, and they discovered that heat transmission is better with cylindrical nanoparticles than spherical nanoparticles. Foukhari et al. [36] explored free convection heat transfer in an annular area within two coaxial cylinders partially filled by a porous medium with a permeable interface and submerged by a nanofluid (Cu–water).

In recent years, the analysis of convection has attracted a growing interest from researchers, who have explored various aspects of convection to gain a deeper understanding of its mechanisms and behaviors. Venkatadri [37] examined the effects of flow in a partially filled porous zone on transverse magnetic flux vectors and heatline visualization. Biswas et al. [38] investigated thermal radiation and chemical reactions using a two-dimensional Maxwell magnetohydrodynamic nanofluid throughout an extended sheet. Venkatadri et al. [39, 40] investigated heat flow visualization in a trapezoidal cavity utilizing energy flux vectors with the impact of thermal radiation as a simulation of high-temperature fuel cell operations. Venkatadri et al. [41] studied several factors for measuring the increase in heat transfer in diverse practical applications by natural convection in porous media. Afikuzzaman et al. [42] used an explicit finite difference approach to analyze an unstable MHD Casson fluid flow across a parallel plate with hall current. Ahmmed et al. [43] demonstrate unstable MHD-natural nanofluid convection motion over an accelerating inclined plate inserted into a porous medium with adjustable thermal conductivity. Afikuzzaman et al. [44] studied the natural convection of a Casson fluid bounded by two parallel non-conducting plates in the presence of a hall current. Venkatadri et al. [45] examined numerically the effect of a baffle on the natural convection of a water-Fe₃O₄ nanofluid in a C-shaped container in the presence of a magnetic field. Rashed et al. [46] looked at the characteristics of nanofluids surrounding a cylinder for laminar steady-state axisymmetric flow. Rashed et al. [47] examined a two-phase model for mixed convection magnetohydrodynamic (MHD) flow combining hybrid nanoparticles, using the Three Parameter Group Transformation Method to simplify the mathematical model. Biswas et al. [48] looked at MHD natural convection and heat transport flux through a vertical porous plate while a chemical reaction was present. Abu-Nab et al. [49] presented the findings of a theoretical model of the growing bubbles at small Mach number in a generalized Newtonian fluid under the influence of magnetic field and shear stress, in which they highlighted the significance of the model's findings for the mechanism of bubble growth in a generalized Newtonian fluid at small Mach number. Over the last two years, there have been a number of studies into the dynamics of bubbles and their behavior in different cases. Abu-bakr et al. [50] examined the behavior of spherical bubbles close to a stiff wall. They concluded that the wall's presence considerably affected bubble growth and caused a considerable difference in the velocities of the interfaces for the both cases: close to and far from the wall. Abu-Nab and Abu-Bakr [51] carefully examined the nonlinear multibubble model while taking into account the interaction between bubbles in a $Cu - Al_2O_3$ /water hybrid nanofluid over the radius of the vapor bubble in Newtonian media. Abu-Nab et al. [52] focused on the theoretical analysis of the pressure relaxation time of N -dimensional spherical bubble dynamics submerged in H₂O/H₂O nanofluid. They demonstrated how the diameter and volume concentration of nanoparticles can both dramatically shorten the time required for pressure relaxation. Shalaby et al. [53] investigated the behavior of a spherical bubble in an N -dimensional fluid composed of vapor and superheated liquid. They demonstrated that as the value of N -dimensions decreases, the radius of the bubble grows. Abu-Nab et al. [54] investigated the influence of heat transmission on the temperature distribution in a superheated liquid during the formation of vapor bubbles immersed in various types of nanoparticles in a two-phase turbulent flow.

The objective of this study was to understand how the process of natural convection works via an annular, partially porous space between two coaxial cylinders with a permeable interface saturated by a Newtonian nanofluid. The simulations discovered provide some insight into potential applications, like the development of new heat exchanger designs. This discovery could lead to the creation of new types of heat exchangers that use natural convection and porous materials to optimize heat transmission. These heat exchangers have potential uses ranging from (heating, ventilation, and air conditioning) systems to industrial operations.

Fig. 1 Physical problem schematic: (a) the 3D geometry (b) the cross section



2 Mathematical formulation

In the current research, we examined an enclosure formed of vertical concentric cylinders with a height of H . The annular space between the two vertical cylinders is partially filled with a porous medium with a thickness of X_p and located on the lateral surface of the inner cylinder Fig. 1. The porous and free regions are saturated by a Newtonian Cu–water nanofluid. The base walls are isolated and impermeable. The inner and outer cylinders are kept at a constant hot and cold temperature, respectively. The flow under consideration is steady in a laminar, incompressible, homogeneous, and isotropic porous medium. The double-domain approach is used in this study to overcome the interface’s restriction on grid localization. The governing equations are formulated based on the formulation of stream function and vorticity under the Boussinesq approximation, [22, 23]. The dimensional governing equations for continuity, momentum, and energy are defined as follows [24].

For the porous layer

$$\frac{1}{r} \frac{\partial(rU)}{\partial r} + \frac{\partial W}{\partial z} = 0, \tag{1}$$

$$\frac{1}{\epsilon^2} \left(\frac{\partial(U\Omega)}{\partial r} + \frac{\partial(W\Omega)}{\partial z} \right) = \frac{\mu_{nf}}{\epsilon \cdot \rho_{nf}} \left(\frac{\partial^2 \Omega}{\partial r^2} - \frac{\Omega}{r^2} + \frac{1}{r} \frac{\partial \Omega}{\partial r} + \frac{\partial^2 \Omega}{\partial z^2} \right) - \frac{\mu_{nf}}{K \cdot \rho_{nf}} \Omega - \beta_{Tnf} \cdot g \frac{\partial T}{\partial r}, \tag{2}$$

$$\frac{\partial(UT)}{\partial r} + \frac{\partial(WT)}{\partial z} + \frac{UT}{r} = \alpha_{eff} \left(\frac{\partial^2 T}{\partial r^2} + \frac{1}{r} \frac{\partial T}{\partial r} + \frac{\partial^2 T}{\partial z^2} \right). \tag{3}$$

For the nanofluid layer

$$\frac{1}{r} \frac{\partial(rU)}{\partial r} + \frac{\partial W}{\partial z} = 0, \tag{4}$$

$$\frac{\partial(U\Omega)}{\partial r} + \frac{\partial(W\Omega)}{\partial z} = \frac{\mu_{nf}}{\rho_{nf}} \left(\frac{\partial^2 \Omega}{\partial r^2} - \frac{\Omega}{r^2} + \frac{1}{r} \frac{\partial \Omega}{\partial r} + \frac{\partial^2 \Omega}{\partial z^2} \right) - \beta_{Tnf} g \cdot \frac{\partial T}{\partial r}, \tag{5}$$

$$\frac{\partial(UT)}{\partial r} + \frac{\partial(WT)}{\partial z} + \frac{UT}{r} = \frac{\partial^2 T}{\partial r^2} + \frac{1}{r} \frac{\partial T}{\partial r} + \frac{\partial^2 T}{\partial z^2}. \tag{6}$$

In order to normalize these governing equations, the following no-dimensional parameters are introduced, for length, velocity, vorticity, stream function, and temperature $(R_e, \frac{\alpha_m}{R_e}, \frac{\alpha_m}{R_e^2}, (\alpha_m \cdot R_e), (T_h - T_c))$, where m refers to nf or eff . However, the nondimensional set of conservation equations can be written as [24]:

For the porous layer

$$\frac{1}{\bar{r}} \frac{\partial(\bar{r}\bar{U})}{\partial \bar{r}} + \frac{\partial \bar{W}}{\partial \bar{z}} = 0, \tag{7}$$

$$\frac{1}{\epsilon^2} \left(\frac{\partial(\bar{U}\bar{\Omega})}{\partial \bar{r}} + \frac{\partial(\bar{W}\bar{\Omega})}{\partial \bar{z}} \right) = \bar{\lambda} \cdot \Gamma \cdot \Sigma \cdot Pr \left(\frac{\partial^2 \bar{\Omega}}{\partial \bar{r}^2} + \frac{1}{\bar{r}} \frac{\partial \bar{\Omega}}{\partial \bar{r}} + \frac{\partial^2 \bar{\Omega}}{\partial \bar{z}^2} \right) + \left(-\bar{\lambda} \cdot \Sigma \frac{Pr}{Da} - \bar{\lambda} \cdot \Gamma \cdot \Sigma \frac{Pr}{\bar{r}^2} \right) \bar{\Omega} - \Lambda \cdot \bar{\lambda}^2 \cdot Ra \cdot Pr \cdot \frac{\partial \bar{T}}{\partial \bar{r}}, \tag{8}$$

$$\frac{\partial(\overline{UT})}{\partial \bar{r}} + \frac{\partial(\overline{WT})}{\partial \bar{z}} + \frac{\overline{UT}}{\bar{r}} = \frac{\partial^2 \bar{T}}{\partial \bar{r}^2} + \frac{1}{\bar{r}} \frac{\partial \bar{T}}{\partial \bar{r}} + \frac{\partial^2 \bar{T}}{\partial \bar{z}^2}. \tag{9}$$

For the nanofluid layer

$$\frac{1}{\bar{r}} \frac{\partial(r\overline{U})}{\partial \bar{r}} + \frac{\partial \overline{W}}{\partial \bar{z}} = 0, \tag{10}$$

$$\frac{\partial(\overline{U\Omega})}{\partial \bar{r}} + \frac{\partial(\overline{W\Omega})}{\partial \bar{z}} = \Sigma \cdot Pr \left(\frac{\partial^2 \overline{\Omega}}{\partial \bar{r}^2} + \frac{1}{\bar{r}} \frac{\partial \overline{\Omega}}{\partial \bar{r}} - \frac{\overline{\Omega}}{\bar{r}^2} + \frac{\partial^2 \overline{\Omega}}{\partial \bar{z}^2} \right) - \Lambda \cdot Ra \cdot Pr \cdot \frac{\partial \bar{T}}{\partial \bar{r}}, \tag{11}$$

$$\frac{\partial(\overline{UT})}{\partial \bar{r}} + \frac{\partial(\overline{WT})}{\partial \bar{z}} + \frac{\overline{UT}}{\bar{r}} = \frac{\partial^2 \bar{T}}{\partial \bar{r}^2} + \frac{1}{\bar{r}} \frac{\partial \bar{T}}{\partial \bar{r}} + \frac{\partial^2 \bar{T}}{\partial \bar{z}^2}. \tag{12}$$

The vorticity function and the velocity fields are defined as:

$$\Omega = \frac{1}{r} \left(\frac{\partial^2 \Psi}{\partial r^2} - \frac{1}{r} \frac{\partial \Psi}{\partial r} + \frac{\partial^2 \Psi}{\partial z^2} \right), \quad \overline{U} = \frac{1}{\bar{r}} \frac{\partial \overline{\Psi}}{\partial \bar{z}}, \quad \overline{W} = -\frac{1}{\bar{r}} \frac{\partial \overline{\Psi}}{\partial \bar{r}}. \tag{13}$$

Where,

$$\Gamma = \frac{\mu^*}{\mu_{nf}}, \quad \alpha_{nf} = \frac{\lambda_{nf}}{(\rho C p)_{nf}}, \quad \alpha_{eff} = \frac{\lambda_{eff}}{(\rho C p)_{nf}}, \quad \bar{\lambda} = \frac{\lambda_{nf}}{\lambda_{eff}}, \tag{14}$$

$$\Sigma = \frac{(1 - \phi)^{-2.5} \left((1 - \phi) + \phi \frac{(\rho C p)_{np}}{(\rho C p)_{bf}} \right)}{\frac{\lambda_{nf}}{\lambda_{bf}} \left((1 - \phi) + \phi \frac{\rho_{np}}{\rho_{bf}} \right)}, \tag{15}$$

$$\Lambda = \frac{\left((1 - \phi) + \phi \frac{(\rho \beta)_{np}}{(\rho \beta)_{bf}} \right)}{\left((1 - \phi) + \phi \frac{\rho_{np}}{\rho_{bf}} \right) \left(\frac{\lambda_{nf}}{\lambda_{bf}} \frac{(\rho C p)_{np}}{(\rho C p)_{bf}} \right)^2}, \tag{16}$$

$$\lambda_{eff} = (1 - \epsilon)\lambda_p + \epsilon\lambda_{nf}. \tag{17}$$

The dimensionless numbers in the above equations are:

$$Ra = \frac{\rho_{bf} g \beta T_h (T_h - T_c) \cdot R_e^3}{\mu_{bf} \alpha_{bf}}, \quad Pr = \frac{\mu_{bf}}{\rho_{bf} \alpha_{bf}}, \quad Da = \frac{k}{R_e^2}. \tag{18}$$

Mahian et al. [25] stated the thermo-physical properties of the nanofluid, which are dependent on both the base fluid and the nanoparticles.

$$\begin{aligned} \rho_{nf} &= (1 - \phi)\rho_{bf} + \phi\rho_{np}, \\ (\rho\beta)_{nf} &= (1 - \phi)(\rho\beta)_{bf} + \phi(\rho\beta)_{np}, \\ (\rho C p)_{nf} &= (1 - \phi)(\rho C p)_{bf} + \phi(\rho C p)_{np}. \end{aligned} \tag{19}$$

The following relationship was provided by Hamilton and Crosser in order to determine a nanofluid’s thermal conductivity [26].

$$\frac{\lambda_{nf}}{\lambda_{bf}} = \frac{\lambda_{np} + (n - 1)\lambda_{bf} + (n - 1)(\lambda_{np} - \lambda_{bf})\phi}{\lambda_{np} + (n - 1)\lambda_{bf} - (\lambda_{np} - \lambda_{bf})\phi}. \tag{20}$$

Brinkman proposed the formula given below to determine the effective viscosity [27].

$$\frac{\mu_{nf}}{\mu_{bf}} = \frac{1}{(1 - \phi)^{-2.5}}. \tag{21}$$

The boundary conditions

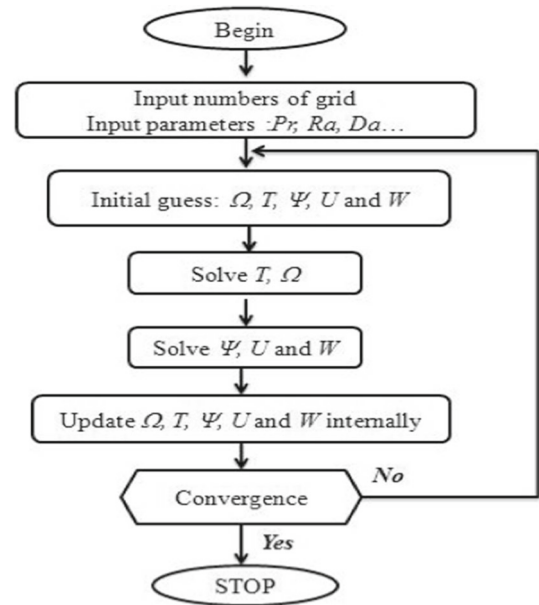
$$\bar{T} = 1, \quad \overline{\Psi} = \frac{\partial \overline{\Psi}}{\partial \bar{r}} = \frac{\partial \overline{\Psi}}{\partial \bar{z}} = 0, \quad \overline{\Omega} = \frac{2}{\Delta \bar{r}^2} \overline{\Psi}|_{\Delta \bar{r}}. \quad \bar{r} = 0.5; \quad 0 \leq \bar{z} \leq AL. \tag{22}$$

$$\bar{T} = 0, \quad \overline{\Psi} = \frac{\partial \overline{\Psi}}{\partial \bar{r}} = \frac{\partial \overline{\Psi}}{\partial \bar{z}} = 0, \quad \overline{\Omega} = \frac{2}{\Delta \bar{r}^2} \overline{\Psi}|_{0.5 - \Delta \bar{r}}. \quad \bar{r} = 1; \quad 0 \leq \bar{z} \leq AL. \tag{23}$$

$$\frac{\partial \bar{T}}{\partial \bar{z}} = 0, \quad \overline{\Psi} = \frac{\partial \overline{\Psi}}{\partial \bar{r}} = \frac{\partial \overline{\Psi}}{\partial \bar{z}} = 0, \quad \overline{\Omega} = \frac{1}{\bar{r}} \frac{2}{\Delta \bar{z}^2} \overline{\Psi}|_{\Delta \bar{z}}. \quad 0.5 \leq \bar{r} \leq 1; \quad \bar{z} = 0. \tag{24}$$

$$\frac{\partial \bar{T}}{\partial \bar{z}} = 0, \quad \overline{\Psi} = \frac{\partial \overline{\Psi}}{\partial \bar{r}} = \frac{\partial \overline{\Psi}}{\partial \bar{z}} = 0, \quad \overline{\Omega} = \frac{1}{\bar{r}} \frac{2}{\Delta \bar{z}^2} \overline{\Psi}|_{AL - \Delta \bar{z}}. \quad 0.5 \leq \bar{r} \leq 1; \quad \bar{z} = AL. \tag{25}$$

Fig. 2 Flow chart for the numerical procedure of solution



The interface conditions are expressed as

$$\begin{cases} \bar{T}_{nf} = \bar{T}_p, & \frac{\partial \bar{T}_{nf}}{\partial \bar{r}} = \frac{\lambda_{eff}}{\lambda_{nf}} \frac{\partial \bar{T}_p}{\partial \bar{r}} \\ \bar{\Psi}_{nf} = \bar{\Psi}_p, & \frac{\partial \bar{\Psi}_{nf}}{\partial \bar{r}} = \frac{\lambda_{eff} \mu_{eff}}{\lambda_{nf} \mu_{nf}} \frac{\partial \bar{\Psi}_p}{\partial \bar{r}} \\ \bar{\Omega}_{nf} = \bar{\Omega}_p, & \frac{\partial \bar{\Omega}_{nf}}{\partial \bar{r}} = \frac{\lambda_{eff} \mu_{eff}}{\lambda_{nf} \mu_{nf}} \frac{\partial \bar{\Omega}_p}{\partial \bar{r}} \end{cases} \quad \text{At } \bar{r} = 0.5 + X_p; 0 \leq \bar{z} \leq AL. \quad (26)$$

The average Nusselt number is used to express the rate of heat transfer coefficient at the active wall, which is given by [55]:

$$Nu_{Average} = \frac{1}{AL} \frac{\lambda_{eff}}{\lambda_{bf}} \int_0^{AL} \frac{\partial \bar{T}_{nf}}{\partial \bar{r}} d\bar{z}. \quad (27)$$

3 Numerical methods

To derive the flow and temperature fields, the sets of dimensionless governing equations associated with the specified boundary conditions are numerically solved, and this comes down to the fact that these problems are characterized by their complexity and nonlinearity. Finite difference discretization is a method used to approximate the solutions of differential equations by discretizing the domain into a finite set of grid points. The governing equations of vorticity and energy are then approximated using the central difference scheme at each grid point. Once the equations have been discretized, the Alternation Direction Implicit (ADI) method is employed to solve the governing algebraic equations, while the stream function equation is solved using the Successive Over Relaxation (SOR) method [28]. This iterative method is a modification of the Gauss-Seidel method, which is used to solve the equations by updating the values of the unknowns at each iteration using a weighted average (typically between 1 and 2). This approach is particularly useful for solving sparse matrices, which often arise from discretizing partial differential equations. The

Table 1 Grid independence test

| Mesh grid | Ra = 10 ⁵ | | Ra = 10 ⁵ | |
|-----------|----------------------|--------|----------------------|--------|
| | Nu _{Aver} | Error% | Nu _{Aver} | Error% |
| 21 × 41 | 4.558 | | 6.970 | |
| 41 × 81 | 4.495 | 1.4 | 6.738 | 3.4 |
| 61 × 121 | 4.478 | 0.37 | 6.676 | 0.9 |
| 71 × 141 | 4.476 | 0.04 | 6.672 | 0.05 |
| 81 × 161 | 4.476 | 0 | 6.67 | 0.02 |

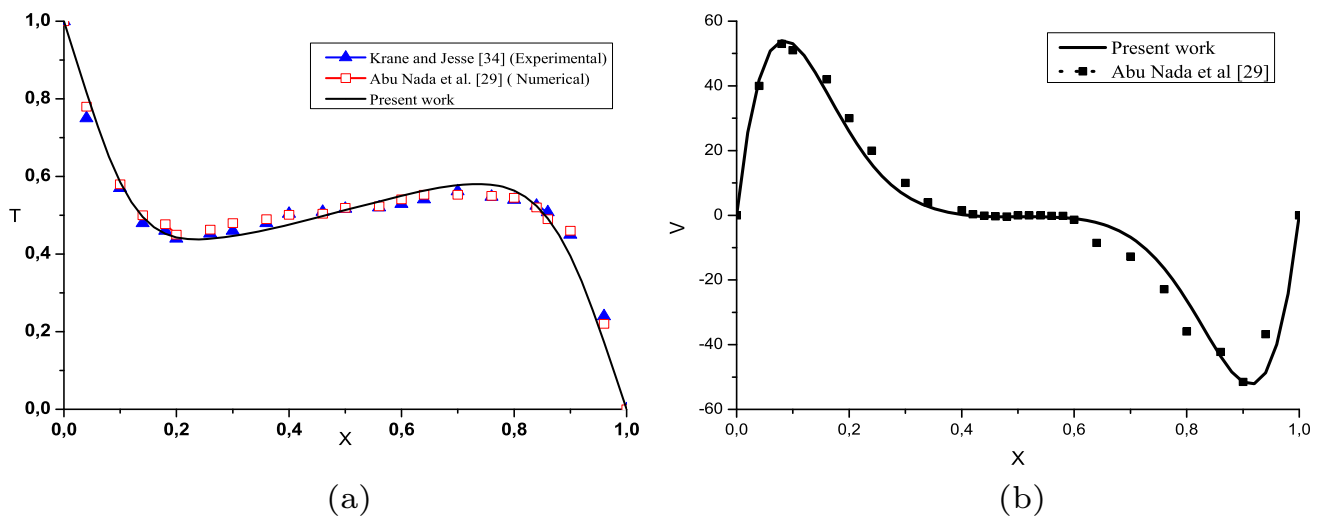


Fig. 3 Comparison of our findings to previous published studies regarding temperature (a) and axial velocity (b) for Al_2O_3 ($Ra = 10^5, Pr = 0.7$)

central difference approximation is used to examine the dynamic field at each grid point for the velocity components. The flow chart of the numerical simulation is shown in Fig. 2. The procedure of iteration was continued until the highest relative change in all dependent variables exceeded the condition.

$$\frac{\sum_i \sum_j |f_{i,j}^{n+1} - f_{i,j}^n|}{\sum_i \sum_j |f_{i,j}^n|} \leq 10^{-5}. \tag{28}$$

Table 1 represents a precision check performed with the finite difference approach and several mesh grid combinations. Nu_{ave} is used to evaluate the grid mesh independence of the current FORTRAN code. It is proven that (61×121) is a good mesh size that assures grid independence.

The current numerical code is validated by comparing our numerical data for $Ra = 10^5$ and $Pr = 0.7$ with numerical data of Abu Nada et al. [29] and experimental data of Krane and Jesse [34] Fig. 3a, 3b, and other data given in the literature Table 2. The interface conditions Eqs. (26) are numerically determined by taking five points, two on the left and two on the right of the interface, and the fifth concentrated at the interface. As a result, the following difference equations are used to compute the interface potentials:

$$\begin{aligned} \overline{\Omega}(i, j) &= \frac{4\overline{\Omega}_{nf}(i + 1, j) - \overline{\Omega}_{nf}(i + 2, j) + \lambda_r \mu_r (4\overline{\Omega}_p(i - 1, j) - \overline{\Omega}_p(i - 2, j))}{3(1 + \lambda_r \mu_r)}, \\ \overline{T}(i, j) &= \frac{4\overline{T}_{nf}(i + 1, j) - \overline{T}_{nf}(i + 2, j) + \lambda_r (4\overline{T}_p(i - 1, j) - \overline{T}_p(i - 2, j))}{3(1 + \lambda_r)}. \end{aligned} \tag{29}$$

Where, $\mu_r = \frac{\mu_{eff}}{\mu_{nf}}$, $\lambda_r = \frac{\lambda_{eff}}{\lambda_{nf}}$ are the effective ratio of dynamic viscosity and thermal conductivity.

4 Results and discussion

The annular space inside two coaxial cylinders with an aspect ratio ($AL = H/R_e$) equal to 2 has been considered for this numerical simulation. This section displays the numerical results in graphical form to demonstrate the effect of the investigated parameters

Table 2 Comparison of the average Nusselt number with other published data for $Pr = 0.7$

| Rayleigh number | 10^4 | | 10^5 | | 10^6 | |
|---------------------------|------------|---------|------------|---------|------------|---------|
| | Nu_{ave} | error % | Nu_{ave} | Error % | Nu_{ave} | Error % |
| Present work | 2.28 | | 4.72 | | 8.393 | |
| Abu Nada et al [29] | 2.244 | 1.6 | 4.644 | 1.63 | 8.862 | 5.58 |
| Del vahl Davis [30] | 2.243 | 1.64 | 4.52 | 4.42 | 8.799 | 4.8 |
| Barakos and Mistolis [31] | 2.23 | 2.24 | 4.51 | 4.65 | 8.806 | 4.84 |
| Fusegi et al [32] | 2.23 | 2.24 | 4.646 | 1.59 | 9.012 | 7.37 |
| Khanafer [33] | 2.245 | 1.55 | 4.522 | 4.37 | 8.826 | 5.15 |

Table 3 Thermo-physical properties of water and Cu [14]

| Properties | Cu | Water |
|---------------------------------|------------------|-----------------|
| ρ [$Kg.m^{-3}$] | 8933 | 997.1 |
| C_p [$J.Kg^{-1}.K^{-1}$] | 385 | 4179 |
| λ [$W.m^{-1}.K^{-1}$] | 401 | 0.613 |
| β [K^{-1}] | $1.67 * 10^{-5}$ | $2.1 * 10^{-5}$ |

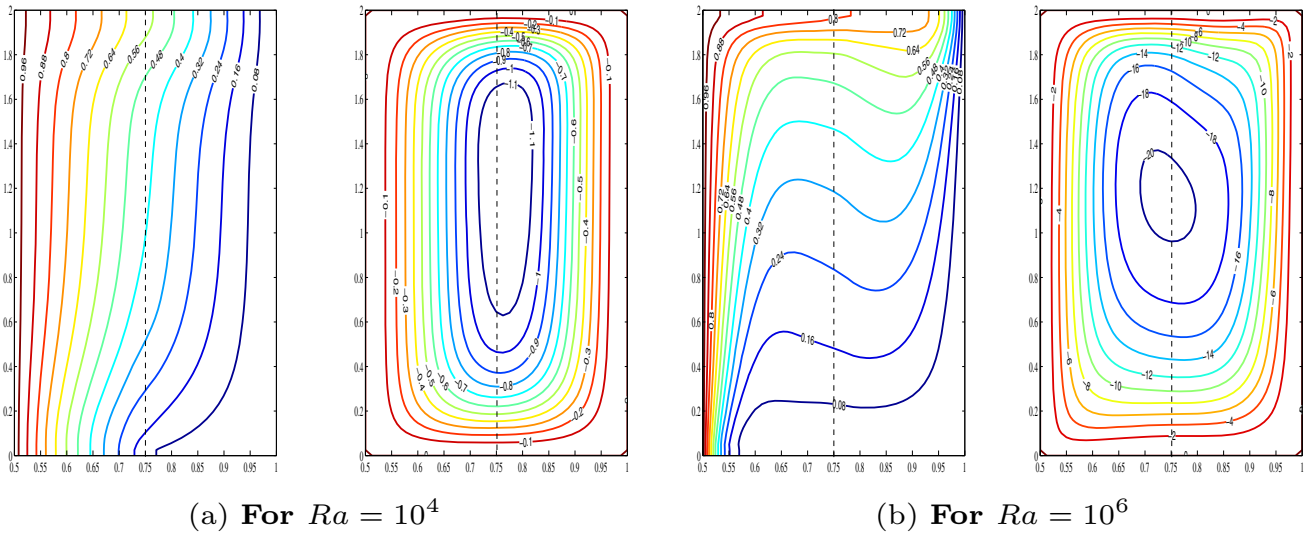


Fig. 4 The isotherms and streamlines at $\phi = 0.05$, $Da = 10^{-2}$ for a) $|\bar{\Psi}| = 1.1977$, b) $|\bar{\Psi}| = 20.4275$

on heat transport. The nanofluid is thought to be made up of water as the base fluid ($Pr = 6.2$) and Cu nanoparticles, as illustrated in Table 3. The porous layer’s porosity is fixed at $\epsilon = 0.7$, which corresponds to glass $\lambda_p = 0.845W/m.K$. The nanoparticle concentration range is $0.01 \leq \phi \leq 0.05$.

Figure 4 displays the distributions of streamlines and isotherms. For $Ra = 10^4$, the entire enclosure is filled with one clockwise circular cell with a low maximum intensity flow, and the isotherms are more compact on the left bottom part, practically vertical. The flow becomes more intense when the Rayleigh number is increased to $Ra = 10^6$ Fig. 4.b. Indeed, a rise in the Rayleigh number may be explained by an increase in the inner cylinder’s heating energy, which causes the nanofluid to escape from the hot side in order to transmit energy to the cold side. We see that the flow on the nanofluid layer is more intense than the porous layer; this is due to the porous layer’s hydrodynamic resistance, which is the consequence of many brakes as friction is created by solid particles in the porous medium.

Figure 5 illustrates the streamlines and isothermal distributions for various Da numbers. For $Da = 10^{-5}$, the isotherms are almost vertical in the lower half, whereas the convection is boosted by an intensity’s flow ($|\bar{\Psi}| = 11.231$). In this state, the fluid moves more slowly within the porous layer, resulting in a slower heat transfer rate. On the other hand, when the Da number increases, the strength of the flow increases Fig. 5.b, which can be explained by the porous media becoming more permeable or decreasing the characteristic diameter of the particles. That’s allowing more nanofluid to pass through the porous layer. While the isotherms become tighter, and the temperature gradient becomes more noticeable when the Darcy number increased to $Da = 0.01$.

The streamlines and isotherm distributions for various porosity levels are shown in Fig. 6. We see that the flow intensity is higher in the free region than in the porous region, and this is due to the localized hydrodynamic resistance in the porous region, which plays an important role as a brake in the flow. Moreover, as the porosity of the medium decreases, the intensity increases, which leads to a rise in the velocity in the free region. To be more understanding, the reduction of the porosity causes most of the fluid to escape to the free zone, while the remaining fluid in the porous region is impeded and mixed owing to the hydraulic resistance of impediments in the porous region. As a result, the velocity in the free zone increases.

Figure 7 depicts the axial velocity component’s radial distribution at the enclosure’s midpoint for various Ra values and various Da numbers. The velocity profile within the porous layer changes from flat to parabolic as the permeability of the porous medium increases, causing a decrease in hydrodynamic resistance. Concerning the Rayleigh number, we can observe that when $Ra = 10^6$, the fluid flow is likely to be dominated by buoyant forces over viscosity, which causes the velocity to increase. Also, the axial velocity is positive in the porous region and negative in the nanofluid region, indicating that the nanofluid rises near the inner cylinder and falls near the outer cylinder; this alternance can be explained by one clockwise cell.

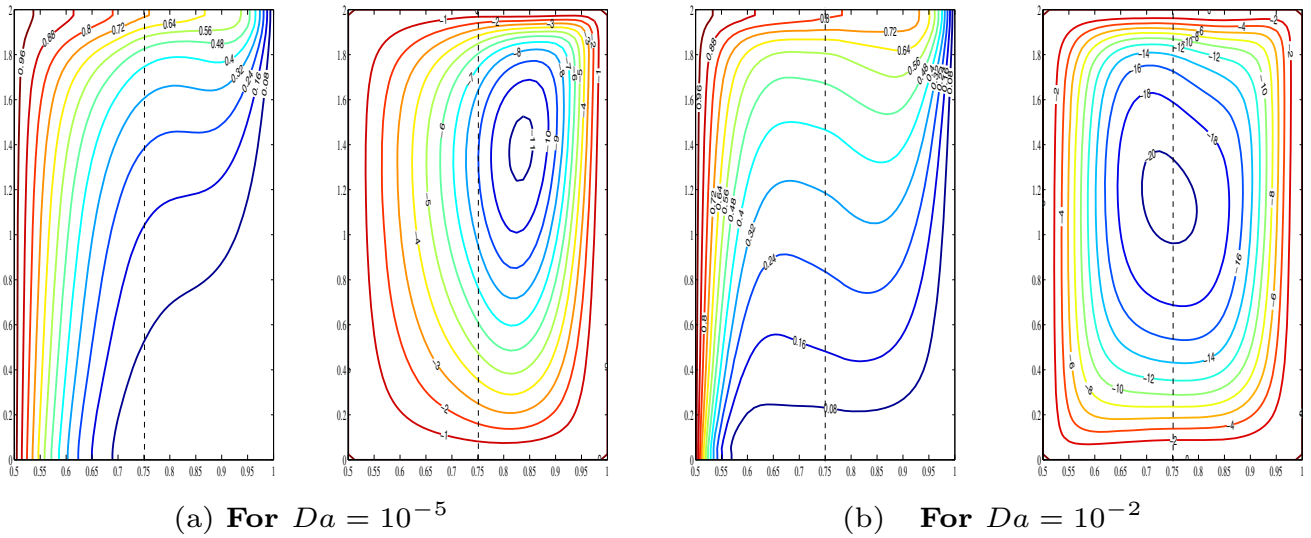


Fig. 5 The isotherms and streamlines at $\phi = 0.05, Ra = 10^6$ for a) $|\bar{\Psi}| = 11.2319$, b) $|\bar{\Psi}| = 20.4275$

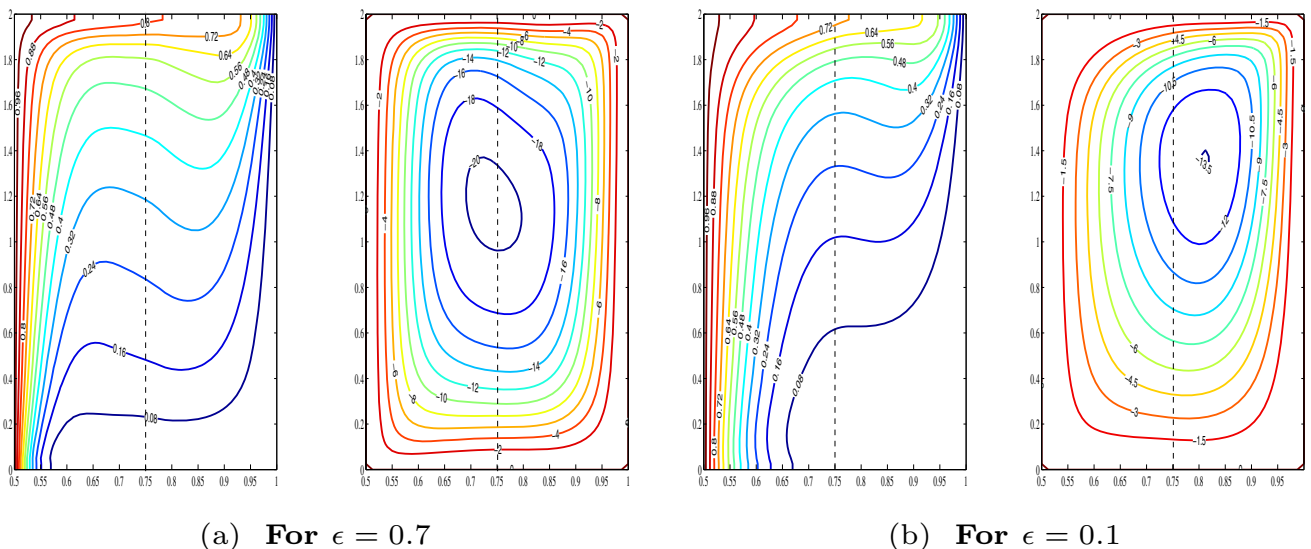


Fig. 6 The isotherms and streamlines at $\phi = 0.05, Ra = 10^6, Da = 10^{-2}$ for a) $|\bar{\Psi}| = 20.4275$, b) $|\bar{\Psi}| = 13.5261$

Fig. 7 Axial velocity's radial distribution for $Pr=6.2, \epsilon = 0.7$ and $\phi = 0.05$

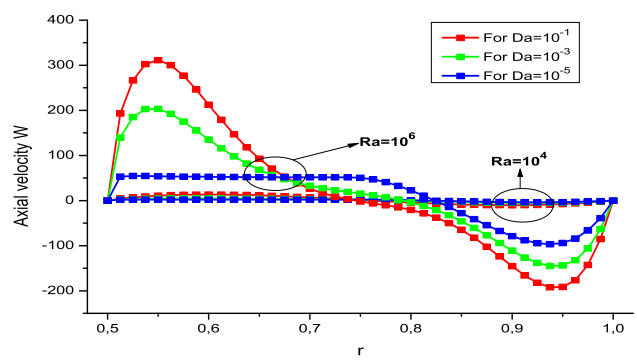


Figure 8a depicts the average Nusselt variation along the inner cylinder for various volume fractions and for different Ra numbers. We can demonstrate from the figure that the average Nusselt number increases when the Rayleigh number increases, as shown in Fig. 4. This increase implies an intensification of fluid motion due to the dominance of buoyant forces, which leads to a more efficient transfer of thermal energy, resulting in a more efficient exchange of heat between the surface and the fluid. We also note the high values of the average Nusselt number for $\phi = 0.05$, indicating the importance of nanoparticle concentration in improving

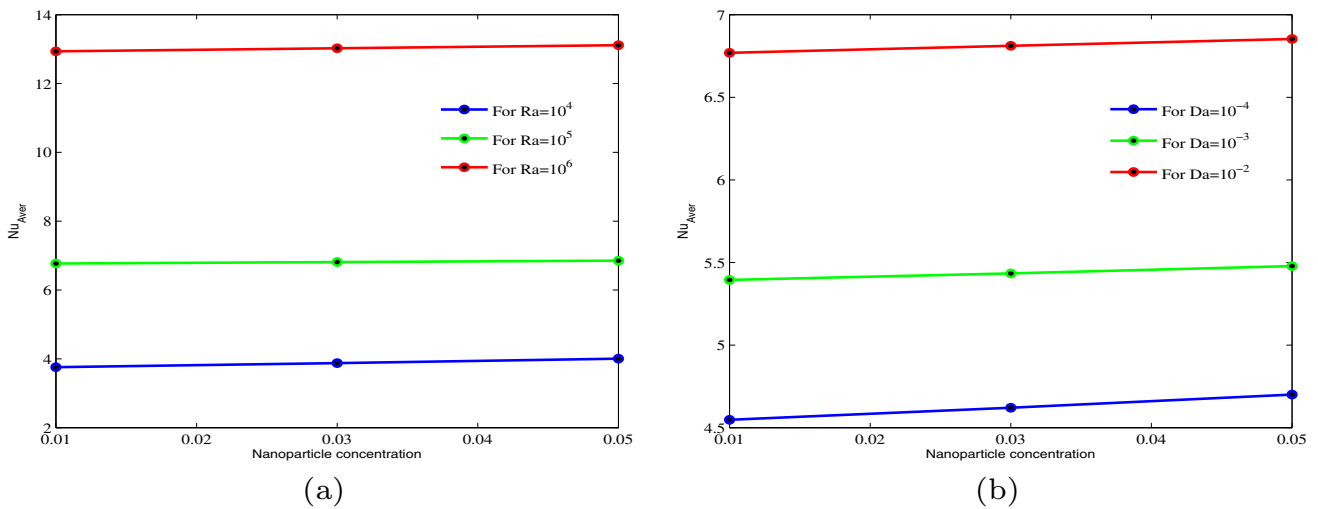
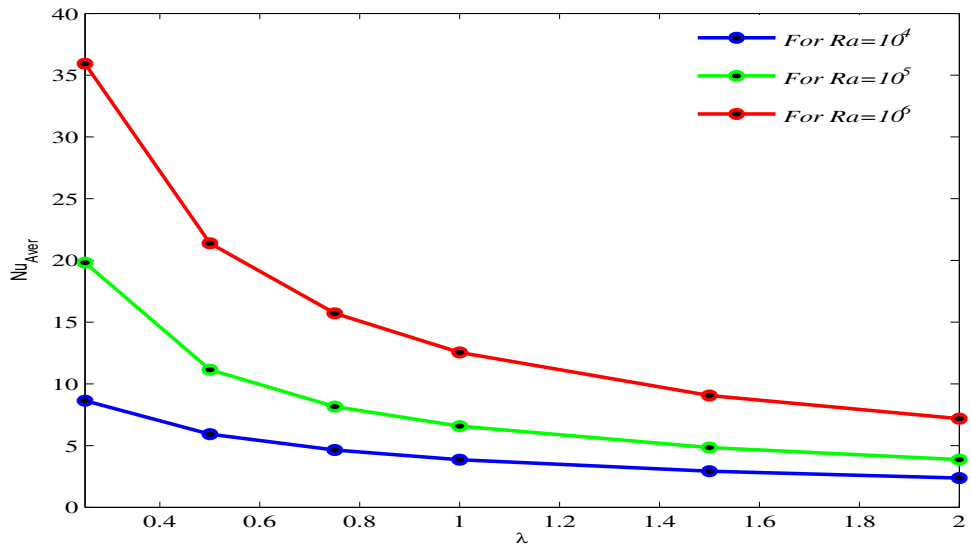


Fig. 8 Some parameters effect on average Nusselt number variation for different Ra and Da numbers at, $\epsilon = 0.7$ for $Da=0.01$ a and $Ra = 10^5$ b

Fig. 9 The effective thermal conductivity ratio effect on average heat transfer for various Rayleigh number for $Da = 10^{-2}$

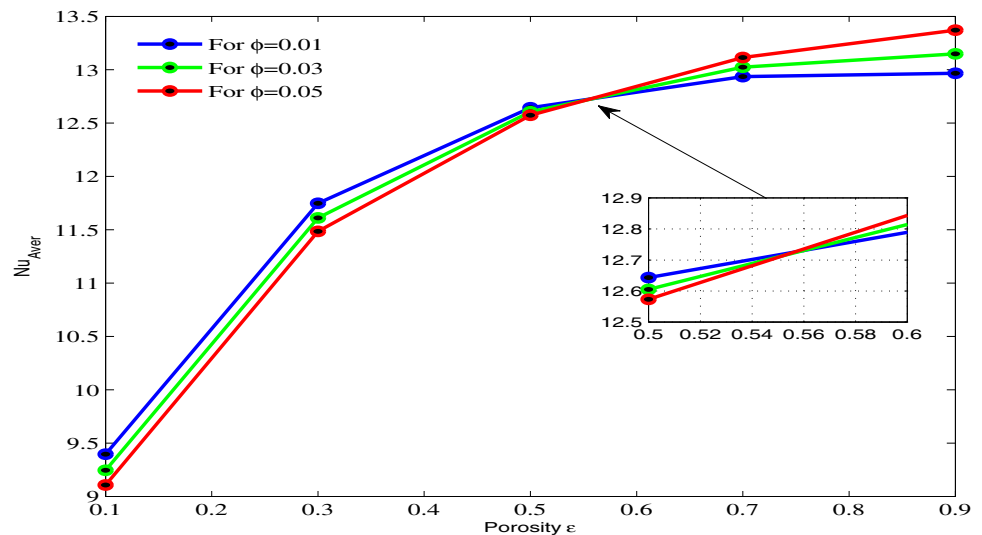


heat transfer. For Fig. 8.b, we can demonstrate that the average Nusselt number rises as the Da number rises, a relationship that may be connected to an increase in permeability. This offers the nanofluid a great deal of freedom, which improves the rate of heat transmission in the active wall. Additionally, it should be noted that high Darcy numbers and nanoparticle volume fraction values result in a higher average Nusselt number.

Figure 9 illustrates the evolution of the Nu_{ave} throughout the inner cylinder for various Rayleigh numbers and different effective thermal conductivity ratio $\bar{\lambda}$. We can observe that the average Nusselt number drops as the effective thermal conductivity ratio grows. That can be explained by the definition of the effective thermal conductivity ratio, which depicts the ratio between the thermal conductivity of the nanofluid and the porous medium that is saturated with the nanofluid. In which, with the drops of this parameter, the thermal conductivity of porous media will be more dominant, thus the heat transfer rate will start to increase, which shows the importance of using a porous material to boost the thermal energy transfer in the active wall.

The evolution of the average Nusselt number around the inner cylinder for various nanoparticle concentrations and various porosity values is shown in Fig. 10. As shown in the graph, the heat transfer rate rises as the porosity number rises. As a result, the flow becomes more intense, and convection becomes more dominant. Furthermore, there is a critical point at which the average Nusselt number increases inversely with increasing nanoparticle concentration; below the critical point, the medium becomes less porous, and the addition of nanoparticles makes the medium more viscous, allowing the conduction mode to dominate. To gain a better understanding, the nanoparticles can fill the spaces between particles in a material, which can increase the material's density and decrease its porosity.

Fig. 10 Porosity effect on heat transfer rate for different nanoparticle concentrations for $Da = 10^{-2}$ and $Ra = 10^6$



5 Conclusion

In this study, we numerically examine the impacts of certain control parameters on fluid flow induced by natural convection heat transfer in an annular zone of concentric cylinders filled with porous media, such as porosity and porous layer thickness. The study region was saturated with a nanofluid made up of Cu nanoparticles and water. The controlled equations are modeled using the finite difference method. Furthermore, the problem was solved using the numerical code FORTRAN, and numerous verification examples were explored using published numerical and experimental data that show great agreement. As a result of the findings, it is possible to conclude:

- The intensity of nanofluid flow circulation improves with increasing Rayleigh number Ra and Darcy number Da , but drops with increasing effective thermal conductivity.
- Because of the porous layer's hydrodynamic resistance, the flow intensity is higher for the nanofluid layer than for the porous layer, as illustrated by the streamlines.
- The rate of thermal energy transfer within the active wall increases as the volume fraction of solid NPs increases.
- The average Nusselt number increases as the porosity increases; there is also a critical point of porosity at which the heat transfer rate increases inversely with the variation in nanoparticle concentration.

Data Availability Statement The datasets generated during and/or analyzed during the current study are available from the corresponding author on reasonable request.

References

1. S.U.S. Choi, Enhancing thermal conductivity of fluids with nanoparticles. Proc. ASME Int. Mech. Eng. Congress Expos. **66**, 99–105 (1995)
2. G.S. Beavers, D.D. Joseph, Boundary conditions at a naturally permeable wall. J. Fluid Mech. **30**(1), 197–207 (1967). <https://doi.org/10.1017/S0022112067001375>
3. Q. Li, R. Zhang, P. Hu, Effect of thermal boundary conditions on forced convection under LTNE model with no-slip porous-fluid interface condition. Int. J. Heat Mass Transf. **167**, 120803 (2021). <https://doi.org/10.1016/j.ijheatmasstransfer.2020.120803>
4. Q. Li, P. Hu, Analytical solutions of fluid flow and heat transfer in a partial porous channel with stress jump and continuity interface conditions using LTNE model. Int. J. Heat Mass Transf. **128**, 1280–1295 (2019)
5. P. Hu, Q. Li, Effect of heat source on forced convection in a partially-filled porous channel under LTNE condition. Int. Commun. Heat. Mass. Transf. **114**, 104578 (2020). <https://doi.org/10.1016/j.icheatmasstransfer.2020.104578>
6. S.A.M. Mehryan, M. Ghalambaz, M. Izadi, Conjugate natural convection of nanofluids inside an enclosure filled by three layers of solid, porous medium and free nanofluid using Buongiorno's and local thermal non-equilibrium models. J. Therm. Anal. Calorim. **135**, 1047–1067 (2019). <https://doi.org/10.1007/s10973-018-7380-y>
7. A.I. Alsabery, A.J. Chamkha, H. Saleh, I. Hashim, B. Chanane, Darcian natural convection in an inclined trapezoidal cavity partly filled with a porous layer and partly with a nanofluid layer. Sains Malays. **46**(5), 803–815 (2017)
8. S. Rashidi, A. Nouri-Borujerdi, M.S. Valipour, R. Ellahi, I. Pop, Stress-jump and continuity interface conditions for a cylinder embedded in a porous medium. Transp. Porous Media. **107**, 171–186 (2015)
9. A.J. Chamkha, A.I. MuneerA, Natural convection in differentially heated partially porous layered cavities filled with a nanofluid. Numer. Heat. Transf. A Appl. **65**(11), 1089–1113 (2014). <https://doi.org/10.1080/10407782.2013.851560>
10. M.A. Sheremet, I. Pop, Natural convection in a horizontal cylindrical annulus filled with a porous medium saturated by a nanofluid using Tiwari and Das' nanofluid model. Eur. Phys. J. Plus. **130**, 107 (2015). <https://doi.org/10.1140/epjp/i2015-15107-4>

11. N. Karimi, Y. Mahmoudi, K. Mazaheri, Temperature fields in a channel partially filled with a porous material under local thermal non-equilibrium condition—an exact solution. *Proc. Inst. Mech. Eng. C J. Mech. Eng. Sci.* **228**(15), 2778–2789 (2014). <https://doi.org/10.1177/0954406214521800>
12. Y. Mahmoudi, N. Karimi, Numerical investigation of heat transfer enhancement in a pipe partially filled with a porous material under local thermal non-equilibrium condition. *Int. J. Heat Mass Transf.* **68**, 161–173 (2014). <https://doi.org/10.1016/j.ijheatmasstransfer.2013.09.020>
13. M.S. Astanina, M.A. Sheremet, H.F. Oztop, N. Abu-Hamdeh, Natural convection in a differentially heated enclosure having two adherent porous blocks saturated with a nanofluid. *Eur. Phys. J. Plus.* **132**, 1–10 (2017). <https://doi.org/10.1140/epjp/i2017-11769-0>
14. A.J. Chamkha, A.I. Muneer, Conjugate heat transfer in a porous cavity filled with nanofluids and heated by a triangular thick wall. *Int. J. Therm. Sci.* **67**, 135–151 (2013). <https://doi.org/10.1016/j.ijthermalsci.2012.12.002>
15. A. Tahmasebi, M. Mahdavi, M. Ghalambaz, Local thermal nonequilibrium conjugate natural convection heat transfer of nanofluids in a cavity partially filled with porous media using Buongiorno's model. *Numer. Heat. Transf. A Appl.* **73**(4), 254–276 (2018). <https://doi.org/10.1080/10407782.2017.1422632>
16. K. Yang, H. Chen, K. Vafai, Investigation of the momentum transfer conditions at the porous/free fluid interface: a benchmark solution. *Numer. Heat. Transf. A Appl.* **71**(6), 609–625 (2017). <https://doi.org/10.1080/10407782.2017.1293977>
17. M. Torabi, N. Karimi, K. Zhang, Heat transfer and second law analyses of forced convection in a channel partially filled by porous media and featuring internal heat sources. *Energy* **93**, 106–127 (2015). <https://doi.org/10.1016/j.energy.2015.09.010>
18. M. Torabi, K. Zhang, G. Yang, J. Wang, P. Wu, Heat transfer and entropy generation analyses in a channel partially filled with porous media using local thermal non-equilibrium model. *Energy* **82**, 922–938 (2015). <https://doi.org/10.1016/j.energy.2015.01.102>
19. A. BaqaieSaryzadi, F. Talebi, T. Armaghani, I. Pop, Numerical study of forced convection flow and heat transfer of a nanofluid flowing inside a straight circular pipe filled with a saturated porous medium. *Eur. Phys. J. Plus.* **131**, 1–11 (2016). <https://doi.org/10.1140/epjp/i2016-16078-6>
20. K. Yang, K. Vafai, Restrictions on the validity of the thermal conditions at the porous-fluid interface—an exact solution. *J. Heat Transf.* **133**(11), 112601 (2011). <https://doi.org/10.1115/1.4004350>
21. A. Bendaraa, M.M. Charafi, A. Hasnaoui, Numerical modeling of natural convection in horizontal and inclined square cavities filled with nanofluid in the presence of magnetic field. *Eur. Phys. J. Plus.* **134**, 468 (2019). <https://doi.org/10.1140/epjp/i2019-12814-8>
22. M. Sammouda, K. Gueraoui, M. Driouich, A. El Hammoumi, A.I. Brahim, The variable porosity effect on the natural convection in a non-Darcy porous media. *Int. Rev. Model. Simul.* (2011). <https://doi.org/10.15866/iremos.v7i2.585>
23. M. Sammouda, K. Gueraoui, MHD double diffusive convection of Al_2O_3 -water nanofluid in a porous medium filled an annular space inside two vertical concentric cylinders with discrete heat flux. *J. Appl. Fluid Mech.* **14**(5), 1459–1468 (2021). <https://doi.org/10.47176/JAFM.14.05.32388>
24. M. Sammouda, K. Gueraoui, M. Driouich, S. Belhouideg, The effect of Al_2O_3 nanoparticles sphericity on heat transfer by free convection in an annular metal-based porous space between vertical cylinders submitted to a discrete heat flux. *J. Porous Media.* **25**(2), (2022). <https://doi.org/10.1615/ComputThermalSci.2021037663>
25. O. Mahian, A. Kianifar, C. Kleinstreuer, A.N. Moh'd A, I. Pop, A.Z. Sahin, S. Wongwises, A review of entropy generation in nanofluid flow. *Int. J. Heat Mass Transf.* **65**, 514–532 (2013)
26. R.L. Hamilton, O.K. Crosser, Thermal conductivity of heterogeneous two-component systems. *Ind. Eng. Chem. Fund.* **1**(3), 187–191 (1962). <https://doi.org/10.1021/i160003a005>
27. H.C. Brinkman, The viscosity of concentrated suspensions and solutions. *J. Chem. Phys.* **20**(4), 571–571 (1952). <https://doi.org/10.1063/1.1700493>
28. M. Sammouda, K. Gueraoui, M. Driouich, A. Ghoulia, A. Dhiri, Double diffusive natural convection in non-darcy porous media with non-uniform porosity. *Int. Rev. Model. Simul.* **7**(6), 1021–1030 (2013).
29. E. Abu-Nada, Z. Masoud, H.F. Oztop, A. Campo, Effect of nanofluid variable properties on natural convection in enclosures. *Int. J. Therm. Sci.* **49**(3), 479–491 (2010). <https://doi.org/10.1016/j.ijthermalsci.2009.09.002>
30. G.D.V. Davis, I.P. Jones, Natural convection in a square cavity: a comparison exercise. *Int. J. Numer. Methods Fluids.* **3**(3), 227–248 (1983). <https://doi.org/10.1002/flid.1650030304>
31. G. Barakos, E. Mitsoulis, D.O. Assimacopoulos, Natural convection flow in a square cavity revisited: laminar and turbulent models with wall functions. *Int. J. Numer. Methods Fluids.* **18**(7), 695–719 (1994). <https://doi.org/10.1002/flid.1650180705>
32. T. Fusegi, J.M. Hyun, K. Kuwahara, B. Farouk, A numerical study of three-dimensional natural convection in a differentially heated cubical enclosure. *Int. J. Heat Mass Transf.* **34**(6), 1543–1557 (1991). [https://doi.org/10.1016/0017-9310\(91\)90295-P](https://doi.org/10.1016/0017-9310(91)90295-P)
33. K. Khanafer, K. Vafai, M. Lightstone, Buoyancy-driven heat transfer enhancement in a two-dimensional enclosure utilizing nanofluids. *Int. J. Heat Mass Transf.* **46**(19), 3639–3653 (2003). [https://doi.org/10.1016/S0017-9310\(03\)00156-X](https://doi.org/10.1016/S0017-9310(03)00156-X)
34. R.J. Krane, Some detailed field measurements for a natural convection flow in a vertical square enclosure. *Proc. First ASME-JSME Therm. Eng. Joint Conf.* **1**, 323–329 (1983)
35. Y. Foukhari, M. Sammouda, M. Driouich, S. Belhouideg, Nanoparticles shape effect on heat transfer by natural convection of nanofluid in a vertical porous cylindrical enclosure subjected to a heat flux. *Int. Conf. Partial Diff. Equ. Appl. Model. Simul.* 437–445 (2023). https://doi.org/10.1007/978-3-031-12416-7_37
36. Y. Foukhari, M. Sammouda, M. Driouich, K. Gueraoui, Heat transfer by natural convection in an annular space partially porous layered and saturated by a nanofluid. *AIP Conf. Proc.* **2761**(1), 040021 (2023)
37. K. Venkatadri, Visualization of thermo-magnetic natural convective heat flow in a square enclosure partially filled with a porous medium using Bejan heatlines and Hooman energy flux vectors: hybrid fuel cell simulation. *Energy Sci. Eng.* **224**, 211591 (2023)
38. R. Biswas, M.S. Hossain, R. Islam, S.F. Ahmed, S.R. Mishra, M. Afikuzzaman, Computational treatment of MHD Maxwell nanofluid flow across a stretching sheet considering higher-order chemical reaction and thermal radiation. *J. Comput. Appl. Math.* **4**, 100048 (2022). <https://doi.org/10.1016/j.jcmds.2022.100048>
39. K. Venkatadri, O.A. Beg, P. Rajarajeswari, V.R. Prasad, Numerical simulation of thermal radiation influence on natural convection in a trapezoidal enclosure: heat flow visualization through energy flux vectors. *Int. J. Mech. Sci.* **171**, 105391 (2020)
40. K. Venkatadri, O. Anwar Béğ, S. Kuharat, Magneto-convective flow through a porous enclosure with Hall current and thermal radiation effects: numerical study. *Eur. Phys. J. Spec. Top.* **231**(13), 2555–2568 (2022)
41. N. Vedavathi, K. Venkatadri, S. Fazuruddin, G.S.S. Raju, Natural convection flow in semi-trapezoidal porous enclosure filled with alumina–water nanofluid using Tiwari and Das' nanofluid model. *Eng. Trans.* **70**(4), 303–318 (2022)
42. M. Afikuzzaman, M. Ferdows, M.M. Alam, Unsteady MHD Casson fluid flow through a parallel plate with hall current. *Proc. Eng.* **105**, 287–293 (2015)
43. S.F. Ahmed, R. Biswas, M. Afikuzzaman, Unsteady magnetohydrodynamic free convection flow of nanofluid through an exponentially accelerated inclined plate embedded in a porous medium with variable thermal conductivity in the presence of radiation. *J. Nanofluids.* **7**(5), 891–901 (2018). <https://doi.org/10.1166/jon.2018.1520>
44. M. Afikuzzaman, M. Ferdows, R.A. Quadir, M.M. Alam, MHD viscous incompressible Casson fluid flow with hall current. *J. Adv. Res. Fluid Mech. Therm. Sci.* **60**(2), 270–282 (2019)

45. K. Venkatadri, A. Shobha, C. Venkata Lakshmi, V. Ramachandra Prasad, B.M. Hidayathulla Khan, Influence of magnetic wire positions on free convection of Fe_3O_4 -water nanofluid in a square enclosure utilizing with MAC Algorithm. *J. Comput. Appl. Mech.* **51**(2), 323–331 (2020)
46. A.S. Rashed, T.A. Mahmoud, A.M. Wazwaz, Axisymmetric forced flow of nonhomogeneous nanofluid over heated permeable cylinders. *Waves Random Complex Media.* 1–29 (2022). <https://doi.org/10.1080/17455030.2022.2053611>
47. A.S. Rashed, S. M. Mabrouk, A.M. Wazwaz, Performance of hybrid two-phase nanofluid neighboring to permeable plates exposed to elevated temperatures. *Waves Random Complex Media.* 1–25(2022). <https://doi.org/10.1080/17455030.2022.2038811>
48. M. Afikuzzaman, R. Biswas, M. Mondal, S. Ahmmed, MHD free convection and heat transfer flow through a vertical porous plate in the presence of chemical reaction. *Front. Heat Mass Transf.* **11**, 11 (2018). <https://doi.org/10.5098/hmt.11.13>
49. A.K. Abu-Nab, M.I. Elgammal, A.F. Abu-Bakr, Bubble growth in generalized-Newtonian fluid at Low-Mach number under influence of magnetic field. *J. Thermophys. Heat Transf.* **36**(3), 485–491 (2022)
50. A.F. Abu-Bakr, T. Kanagawa, A.K. Abu-Nab, Analysis of doublet bubble dynamics near a rigid wall in ferroparticle nanofluids. *Case Stud. Therm. Eng.* **34**, 102060 (2022). <https://doi.org/10.1016/j.csite.2022.102060>
51. A.K. Abu-Nab, A.F. Abu-Bakr, Effect of bubble–bubble interaction in $\text{Cu-Al}_2\text{O}_3/\text{H}_2\text{O}$ hybrid nanofluids during multibubble growth process. *Case Stud. Therm. Eng.* **33**, 101973 (2022)
52. A.K. Abu-Nab, M.H. Omran, A.F. Abu-Bakr, Theoretical analysis of pressure relaxation time in N -dimensional thermally-limited bubble dynamics in Fe_3O_4 /water nanofluids. *J. Nanofluids.* **11**(3), 410–417 (2022)
53. G.A. Shalaby, A.F. Abu-Bakr, Growth of N -dimensional spherical bubble within viscous, superheated liquid: analytical solution. *Therm. Sci.* **25**, 504–514 (2021)
54. A.K. Abu-Nab, A.F. Abu-Bakr, Effect of heat transfer on the growing bubble with the nanoparticles/water nanofluids in turbulent flow. *Math. Model. Eng.* **8**(1), 95–102(2021). <https://doi.org/10.18280/mmep.080112>
55. K.D. Singh, R. Kumar, Fluctuating heat and mass transfer on unsteady MHD free convection flow of radiating and reacting fluid past a vertical porous plate in slip-flow regime. *J. Appl. Fluid Mech.* **4**(4) 101–106 (2012). <https://doi.org/10.36884/jafm.4.04.11952>

Springer Nature or its licensor (e.g. a society or other partner) holds exclusive rights to this article under a publishing agreement with the author(s) or other rightsholder(s); author self-archiving of the accepted manuscript version of this article is solely governed by the terms of such publishing agreement and applicable law.